Universal method to determine the thermo-optic coefficient of optical waveguide layer materials using a dual slab waveguide

David R. Cassidy and Graham H. Cross[a)]
Department of Physics, Durham University, South Road, Durham DH1 3LE, United Kingdom

(Received 7 June 2007; accepted 17 September 2007; published online 3 October 2007)

A dual slab waveguide device method for determining the thermo-optic coefficient of waveguide layer materials is demonstrated. Temperature change-induced optical path length imbalance between two single slab waveguide modes provides the primary mechanism for detection. The waveguide mode output field phase change differences are encoded in shifts in the far field interference pattern. To illustrate the method, the thermo-optic coefficients of two $In_{1-x}Ga_xAs_yP_{1-y}$ quaternary alloys, 1.3*Q* and 1.15*Q*, are measured at a wavelength of 1.55 μm and at a center temperature of 25.2 °C. Their ratio is in excellent agreement with previous work, in accordance with optical dispersion models. © *2007 American Institute of Physics*. [DOI: 10.1063/1.2795340]

An understanding of the thermal behavior of guided wave photonic devices is crucial; whether one is designing a device where this behavior provides the device functionality[1] or whether it is a problem to be managed.[2] The intrinsic thermal response of a device (as opposed to extrinsic sources due to the packaging) can be modeled accurately provided that the thermo-optic coefficients of the materials comprising the device are known. For many common optical materials such as silica lithium niobate, silicon, and other semiconductor crystals such as the III-V binaries (InP, GaAs, etc.), these coefficients are now described well by the pioneering dispersion model of Ghosh.[3] Experimental verification of thermo-optic coefficients, however, requires suitable sample geometries such as a prism[4] or etalon[5] or integrated optical waveguide device,[6] and in part for this reason, there is a scarcity (essentially an absence) of the reported thermo-optic coefficients of materials of the quaternary III-V compound semiconductors. These alloys are not formed as bulk crystals but as thin epitaxial layers by metal organic vapor phase epitaxy (MOVPE) growth on the binary alloy crystal wafer substrate. Despite the obviously successful development of vital optoelectronic components (for example, diode lasers and photodetectors) that use quaternary materials, designers would benefit from having access to such data and we provide here a device-based method that is relatively simple to implement that allows the measurement, in principle, of any desired III-V alloy system across wide ranges of temperatures and wavelengths. We report the thermo-optic coefficient for two InGaAsP compositions at the wavelength center of the ITU *C* band $\lambda_0 = 1.55$ μm and at a center temperature of 25.2 °C.

We previously demonstrated an InP/InGaAsP dual slab waveguide unbalanced interferometer designed to detect picometer level changes in *C*-band laser wavelength.[7,8] The interferometer consists very simply of five epitaxial layers of alternately low and high refractive indices (here, InP and InGaAsP, respectively) fabricated on suitable absorbing layers and on a heavily doped InP substrate (see Table I and the inset of Fig. 1). End fire of an oversized optical field into the waveguide sample excites both single slab modes with equal efficiency. All nonguided light is either absorbed into the lower layers or scattered through the device surface.[9] At the device output, the two modes diffract into the far field at the output plane where they form a clear interference pattern analogous to Young's fringes (Fig. 1). The spatial intensity distribution of the fringe pattern provides information on the relative phase difference, between the "upper" (u) and "lower" (l) waveguide fields at the output plane of the device, reflecting the difference in effective refractive index, $N_{u(l)}$ between the modes.Thickness and compositional differences between the two guiding layers produce a difference in the effective thermo-optic coefficient $dN_{u(l)}/dT$ of the two modes. As the temperature changes ΔT, the net effect is an output phase change difference $\Delta\Phi$ related to the effective index change between the modes and change in sample length due to thermal expansion given by

$$\Delta\Phi = \frac{2\pi}{\lambda_0} L\Delta T[dN_u/dT - dN_l/dT + \alpha(N_u - N_l) + \alpha\Delta T(dN_u/dT - dN_l/dT)], \quad (1)$$

where L is the length of the interferometer chip and α is the

TABLE I. Device layer structure with alternative layer 6 for the 1.3*Q* (a) and 1.15*Q* (b) designs. The measured photoluminescence wavelengths (λ_g) of the ternary and quaternary materials are given in parentheses.

Layer	Material	Dopant	Thickness (μm)	n (1.55 μm)
Substrate	2 in. InP VCz	S	350	···
1	InP	Si	0.5	···
2	InGaAs (λ_g=1.65 μm)	···	1.0	···
3	InP	···	1.5	3.1836
4	1.3*Q* InGaAsP (λ_g=1.290 μm)	···	0.5	3.3907(8)
5	InP	···	2.3	3.1836
6(a)	1.3*Q* InGaAsP (λ_g=1.290 μm)	···	0.2	3.3907(8)
6(b)	1.15*Q* InGaAsP (λ_g=1.155 μm)	···	0.3	3.3206(4)
7	InP	···	2.0	3.1836

[a)]Electronic mail: g.h.cross@durham.ac.uk

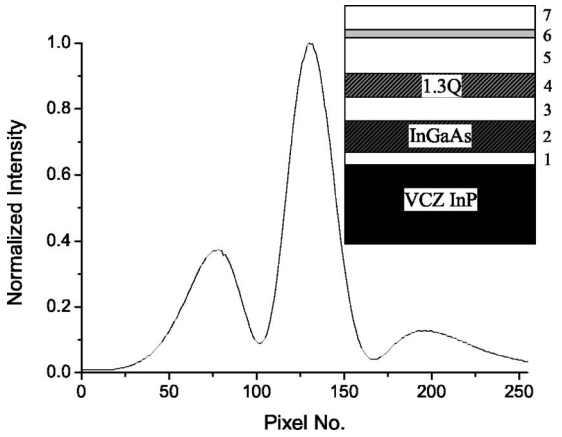

FIG. 1. Representative fringe image on the linear photodiode array. The inset is a schematic diagram of the dual slab layer system corresponding to the properties shown in Table I.

effective thermal expansion coefficient. In practice, the final summation term in parentheses is vanishingly small and will be neglected. The central term will make a small correction and will be retained. The effective thermal expansion coefficient will be taken to be that for bulk InP ($\alpha = +4.56 \times 10^{-6}\ \mathrm{K}^{-1}$) given that the layers are epitaxial to this wafer substrate. Any stress-optical effects cannot be accounted for.

Each symmetrical slab waveguide is a high confinement system (see Fig. 2) and can be considered in isolation in which case the effective refractive index $N_{u(l)}$ of the waveguiding modes can be expressed simply as a function of the refractive index of the three layers it propagates through. The index of each layer is itself a function of temperature and as such, following the chain rule, the effective thermo-optic coefficient, $dN_{u(l)}/dT$ of each mode can be expressed as a summation of the following partial derivatives:

$$\frac{dN_{u(l)}}{dT} = \frac{\partial N_{u(l)}}{\partial n_1}\frac{dn_1}{dT} + \frac{\partial N_{u(l)}}{\partial n_2}\frac{dn_2}{dT} + \frac{\partial N_{u(l)}}{\partial n_3}\frac{dn_3}{dT}, \tag{2}$$

where $dn_{1(2,3)}/dT$ is the thermo-optic coefficient of the corresponding layer and $\partial N_{u(l)}/\partial n_{1(2,3)}$ is a measure of the rate of change of effective mode index with layer index found by calculating $N_{u(l)}$ against individual changes in $n_{1(2,3)}$ over a very small range of refractive index around the reported nominal values.

For these symmetric slab waveguides, the effective thermo-optic coefficient can be simplified to

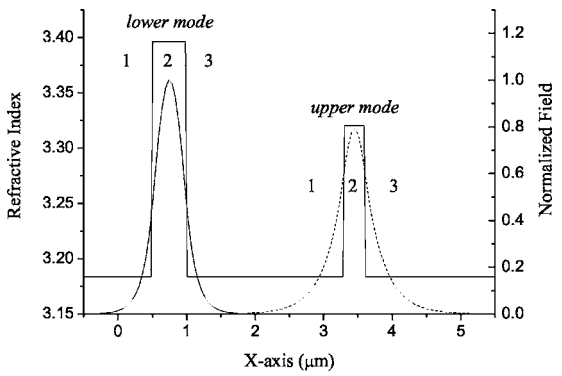

FIG. 2. Transverse optical field amplitude distribution and refractive index profile for the $1.3Q/1.15Q$ structure whose properties are listed in Table I.

$$\frac{dN_{u(l)}}{dT} = 2\frac{\partial N_{u(l)}}{\partial n_{\mathrm{InP}}}\frac{dn_{\mathrm{InP}}}{dT} + \frac{\partial N_{u(l)}}{\partial n_{Qu(Ql)}}\frac{dn_{Qu(Ql)}}{dT}, \tag{3}$$

where $dn_{Qu(Ql)}/dT$ is the thermo-optic coefficient of the quaternary waveguide layer material. Using this definition in Eq. (1) leads to

$$\frac{\partial N_u}{\partial n_{Qu}}\frac{dn_{Qu}}{dT} - \frac{\partial N_l}{\partial n_{Ql}}\frac{dn_{Ql}}{dT} = \frac{\lambda_0 \Delta\Phi}{2\pi L \Delta T} - \left(2\frac{\partial N_u}{\partial n_{\mathrm{InP}}} - 2\frac{\partial N_l}{\partial n_{\mathrm{InP}}}\right)\frac{dn_{\mathrm{InP}}}{dT} - \alpha(N_u - N_l). \tag{4}$$

For an interferometer where the quaternary alloy is identical ($1.3Q$) in upper and lower slab waveguides, we have

$$\frac{dn_{1.3Q}}{dT} = \left[\frac{\lambda_0 \Delta\Phi}{2\pi L \Delta T} - \left(2\frac{\partial N_u}{\partial n_{\mathrm{InP}}} - 2\frac{\partial N_l}{\partial n_{\mathrm{InP}}}\right)\frac{dn_{\mathrm{InP}}}{dT} - \alpha(N_u - N_l)\right] \Bigg/ \left(\frac{\partial N_u}{\partial N_{Qu}} - \frac{\partial N_l}{\partial n_{Ql}}\right), \tag{5}$$

and a rearrangement of Eq. (3) provides a similar equation for the dual quaternary system [structure (b)] where the unknown ($1.15Q$) quaternary material is in the upper waveguide,

$$\frac{dn_{1.15Q}}{dT} = \left[\frac{\lambda_0 \Delta\Phi}{2\pi L \Delta T} - \left(2\frac{\partial N_u}{\partial n_{\mathrm{InP}}} - 2\frac{\partial N_l}{\partial n_{\mathrm{InP}}}\right)\frac{dn_{\mathrm{InP}}}{dT} + \frac{\partial N_l}{\partial n_{Ql}}\frac{dn_{1.3Q}}{dT} - \alpha(N_u - N_l)\right] \Bigg/ \frac{\partial N_u}{\partial N_{Qu}}. \tag{6}$$

Thus, we can determine the thermo-optic coefficient for the quaternary materials from the measured phase changes provided that we have a reliable value for the thermo-optic coefficient of InP. An acceptable value, $dn_{\mathrm{InP}}/dT = (+1.95 \pm 0.05) \times 10^{-4}\ \mathrm{K}^{-1}$, was taken from the average results of a range of published experimental measurements[4–6,10] carried out at or near 1.55 μm and at 25 °C.

Two structures were fabricated using $1.3Q$ material for both guiding layers in one design (a) and guiding layers of each of $1.3Q$ and $1.15Q$ materials in the other (b) (Table I). The experimentally determined photoluminescence wavelengths were taken to indicate the position of the band gap for the quaternary materials, and refractive index values for these layers at 1550 nm were obtained using the formulas of Adachi[11] built into the FIMMWAVE© program of Photon Design.[12] The calculated values of $\partial N_{u(l)}/\partial n_{\mathrm{InP}}$ and $\partial N_{u(l)}/\partial n_{Qu(Ql)}$ are given in Table II.

Devices were cleaved into a length of 12 mm and a width of 2 mm. The interferometer chip was clamped within a dual-stage temperature-controlled housing with Peltier control to better than ±5 mK for the sample. The input light was provided by an Agilent 81640A tuneable laser source coupled into a standard single mode optical fiber wound onto a polarization controller allowing both transverse electric (TE) and transverse magnetic (TM) polarized excitations of the modes.

The cleaved bare fiber output facet was positioned near to the interferometer chip end face in order for the light to diffract to a beam size sufficient to excite both waveguiding modes with approximately equal efficiency. In order to prevent uncoupled and scattered light from reaching the detec-

TABLE II. Calculated rate of change of effective mode index with layer index for $1.3Q$ [structure (a)] and $1.3Q/1.15Q$ [structure (b)] devices.

	Structure (a)		Structure (b)	
	TE	TM	TE	TM
$\frac{\partial N_u}{\partial n_{Qu}}$	0.3264	0.2550	0.4121	0.3586
$\frac{\partial N_l}{\partial n_{Ql}}$	0.7678	0.7136	0.7678	0.7137
$2\frac{\partial N_u}{\partial n_{\mathrm{InP}}}$	0.6820	0.7544	0.5946	0.6489
$2\frac{\partial N_l}{\partial n_{\mathrm{InP}}}$	0.2456	0.3027	0.2455	0.3027

tor, it is necessary to grow the five-layer dual waveguide structures (layers 3–7) on top of a layer of low band gap ternary material which absorbs any light radiating out of the confinement layers. This layer is separated from the lower interferometer waveguide mode such that the absorption loss is less than 0.1 dB/cm. To prevent direct transmission through the substrate, a Si-doped ($N=1\times10^{18}$ cm^{-3}) InP layer is deposited on top of a highly absorbing S-doped ($N=5\times10^{18}$ cm^{-3}) InP substrate. These precautions ensure that the output light from the device end facet is from waveguiding modes only and allow for a highly visible fringe pattern to be formed in the far field.

The interference pattern falls onto a 256 pixel InGaAs linear array (Hamamatsu C8061) and data are collected via a computer interface. Pixel voltages are read into a discrete Fourier transform algorithm to produce a relative phase difference value for the two source fields. The calculated phase values are insensitive to input optical power fluctuations, and the overall noise floor of the device is ±1 mrad.

The temperature was stepped across a full range of 400 mK (25.0–25.4 °C), and at each step, a dwell time of greater than 15 min was included to allow the equipment and sample temperature to settle. Mean values of the response were obtained from repeated measurements. The mean sensitivity to temperature change around 25 °C for the $1.3Q$ interferometer chip [structure (a)] at a fixed wavelength of 1.55 μm was measured as $\Delta\Phi_{\mathrm{TE}}/\Delta T=-2.705\pm0.15$ rad K^{-1} and $\Delta\Phi_{\mathrm{TM}}/\Delta T=-2.7114\pm0.15$ rad K^{-1}. For the $1.3Q/1.15Q$ design [structure (b)], the mean thermal sensitivities found were $\Delta\Phi_{\mathrm{TE}}/\Delta T=-3.240\pm0.23$ rad K^{-1} and $\Delta\Phi_{\mathrm{TM}}/\Delta T=-3.179\pm0.13$ rad K^{-1}.

The thermo-optic coefficients, calculated using these values in Eqs. (5) and (6), are shown in Table III. They lie above the thermo-optic coefficients of InP (1.95×10^{-4} K^{-1}) and GaAs (2.35×10^{-4} K^{-1}) (Ref. 5) and, as would be expected because of the dispersion effects,[3] the lower band gap material has a larger thermo-optic coefficient. Although there is little to compare with in the literature, the ratio between the two coefficients is, however, in excellent agreement with the results of a previous device study[13] which reported a ratio of 0.81 between the thermo-optic coefficients of $1.1Q$ and $1.3Q$.

TABLE III. Thermo-optic coefficients of $1.3Q$ and $1.15Q$ alloys determined at TE and TM excitations at a wavelength of 1.55 μm and at a center temperature of 25.2 °C.

	$1.3Q$ ($\lambda_g=1.290$ μm) (K^{-1})	$1.15Q$ ($\lambda_g=1.155$ μm) (K^{-1})	Ratio ($1.15Q/1.3Q$)
dn/dT (TE)	$(3.18\pm0.18)\times10^{-4}$	$(2.62\pm0.19)\times10^{-4}$	0.823
dn/dT (TM)	$(3.13\pm0.17)\times10^{-4}$	$(2.58\pm0.11)\times10^{-4}$	0.825

In conclusion, we have demonstrated a method for determining the thermo-optic coefficients of MOVPE-deposited InGaAsP layers to a high accuracy. Very simple device structures, requiring only epitaxial multilayer deposition and no lithography, are described. The present studies are limited to reporting values at a wavelength of 1.55 μm and at a temperature of 25 °C, but this technique could be readily extended to cover the wavelength and temperature space required by device engineers.

This work was supported by the UK EPSRC through a studentship to David Cassidy and with epilayer fabrication at the EPSRC National III-V Centre in Sheffield, UK.

[1] C. Y. Wu, P. Lin, R.-S. Huang, W.-C. Chao, and M. M. H. Lee, Appl. Phys. Lett. **89**, 121121 (2006).
[2] M. Yan, T. S. Tarter, J. Weaver, X. Hao, and C. K. Ho, IEEE Trans. Compon. Packag. Technol. **28**, 667 (2005).
[3] G. Ghosh, *Handbook of Thermo-Optic Coefficients of Optical Materials with Applications* (Academic, New York, 1998), Chap. 3, p. 115.
[4] M. Bertolotti, V. Bogdanov, A. Ferrari, A. Jascow, N. Nazorova, A. Pikhtin, and L. Schirone, J. Opt. Soc. Am. B **7**, 918 (1990).
[5] F. G. Della Corte, G. Cocorullo, M. Iodice, and I. Rendina, Appl. Phys. Lett. **77**, 1614 (2000).
[6] E. Gini and H. Melchior, J. Appl. Phys. **79**, 4335 (1996).
[7] G. H. Cross and E. E. Strachan, IEEE Photonics Technol. Lett. **14**, 950 (2002).
[8] D. R. Cassidy and G. H. Cross, IEEE Photonics Technol. Lett. **19**, 1075 (2007).
[9] G. H. Cross, Y. Ren, and N. J. Freeman, J. Appl. Phys. **86**, 6483 (1999).
[10] P. Martin, E. M. Skouri, L. Chusseau, and C. Alibert, Appl. Phys. Lett. **67**, 881 (1995).
[11] S. Adachi, J. Appl. Phys. **58**, R1 (1985).
[12] See www.photond.com for FIMMWAVE optical waveguide modeling software.
[13] H. Tanobe, Y. Kondo, Y. Kadota, H. Yasaka, and Y. Yoshikuni, IEEE Photonics Technol. Lett. **8**, 1489 (1996).